REPORT DOCUMENTATION PAGE

Form Approved
OMB No. 0704-0188

1. REPORT DATE *(DD-MM-YYYY)*	2. REPORT TYPE	3. DATES COVERED *(From - To)*
31-12-2011	Performance/Technical Report (Final)	Jan. 2009 - Dec. 2011

4. TITLE AND SUBTITLE
Enhanced Multistatic Active Sonar via Innovative Signal Processing

5a. CONTRACT NUMBER

5b. GRANT NUMBER
N00014-09-1-0211

5c. PROGRAM ELEMENT NUMBER

6. AUTHOR(S)
Jian Li

5d. PROJECT NUMBER

5e. TASK NUMBER

5f. WORK UNIT NUMBER

7. PERFORMING ORGANIZATION NAME(S) AND ADDRESS(ES)
University of Florida
Office of Engineering Research
343 Weil Hall, P.O.Box 116550
Gainesville, FL 32611

8. PERFORMING ORGANIZATION REPORT NUMBER

9. SPONSORING/MONITORING AGENCY NAME(S) AND ADDRESS(ES)
Office of Naval Research
875 North Randolph Street
Arlington, VA 22203-1995

10. SPONSOR/MONITOR'S ACRONYM(S)
ONR

11. SPONSORING/MONITORING AGENCY REPORT NUMBER

12. DISTRIBUTION AVAILABILITY STATEMENT
Approved for Public Release; Distribution is Unlimited.

13. SUPPLEMENTARY NOTES

14. ABSTRACT
Multistatic active sonar systems involve the transmission and reception of one or more probing sequences, which provide a basis for extraction of target information in a region of interest. The probing sequences at the transmitter and signal processing at the receiver play crucial roles in the overall system performance. CAN (cyclic algorithm-new) is employed to synthesize probing sequences with good aperiodic autocorrelation properties. The performance of the CAN sequences is compared with those of pseudo random noise and random phase sequences. Two adaptive receiver designs, namely the iterative adaptive approach (IAA) and the sparse learning via iterative minimization (SLIM) method, are also considered. IAA and SLIM are compared with the conventional matched filter method. The performances of the algorithms are illustrated via numerical examples, which show that CAN, IAA, and SLIM can contribute to the overall performance improvement of the active sonar systems.

15. SUBJECT TERMS
Multistatic active sonar system, probing sequence, cyclic algorithm-new, adaptive receiver design, iterative adaptive approach, sparse learning via iterative minimization

16. SECURITY CLASSIFICATION OF:			17. LIMITATION OF ABSTRACT	18. NUMBER OF PAGES	19a. NAME OF RESPONSIBLE PERSON
a. REPORT	b. ABSTRACT	c. THIS PAGE	UU	17	Jian Li
U	U	U			19b. TELEPONE NUMBER *(Include area code)* (352) 392-2642

Enhanced Multistatic Active Sonar via Innovative Signal Processing

Jian Li
Department of Electrical and Computer Engineering, P.O. Box 116130
University of Florida, Gainesville, FL 32611
phone: (352) 392-2642 fax: (352) 392-0044 email: li@dsp.ufl.edu

Award Number: N00014-09-1-0211
http://www.sal.ufl.edu

LONG-TERM GOALS

Our goal is to address fundamental signal processing research issues for enhanced multistatic active sonar systems. To effectively mitigate the reverberation problems encountered in shallow water, both probing waveform synthesis and receive filter design need to be optimized.

OBJECTIVES

Our objectives are 1) to optimally synthesize broadband Doppler-sensitive probing waveforms under practical (e.g., constant modulus and total energy) constraints, and 2) to devise robust and computationally efficient receive filters including data-independent mismatched filters as well as data-dependent sparse signal representation algorithms for superior range-Doppler (or angle-range-Doppler) imaging. Our goal is to significantly reduce the shallow water reverberation effects on the detection of both high- and low-Doppler targets. The interplay between the probing waveform synthesis and receive filter design on the performance of the multistatic active sonar systems will be investigated as well.

APPROACH

For Doppler-sensitive probing waveform synthesis, we consider optimizing the integrated sidelobe level (ISL) metric. Lower ISL means lower sidelobe levels after range compression, which in turn means lower interferences among scatterers located at different range bins. Due to hardware constraints (such as the limitations of the power amplifier) in practice, components of the transmitted waveform are commonly restricted to being constant modulus. Our goal is to minimize the ISL metric over the set of unimodular (i.e., unit modular) sequences. Note that the minimization of the ISL metric is equivalent to the maximization of the well-known merit factor (MF) discussed in the literature.

The probing waveforms we synthesize can never be perfect, as dictated by fundamental performance bounds and principles. In general, the ambiguity functions can never be made like a perfect thumb-tack. Fortunately, novel receiver design techniques can serve to improve the overall performance of the active sonar system and can be used to compensate for the deficiencies in waveform synthesis. For receive filter design, we consider matched, mismatched, and adaptive filters to form range-Doppler or angle-range-Doppler images. The adaptive filters, in particular, will be developed to significantly

reduce the mutual interferences of scatterers in different range and Doppler bins and to improve the Doppler resolution.

The key individuals participating in this work include the PI, Jian Li, and her Ph.D. students, Hao He, Jun Ling, and William Roberts, at the University of Florida, as well as Professor Petre Stoica at the Uppsala University in Sweden. Dr. He has been funded as a Research Associate (RA) by this ONR grant and he has received his Ph.D. degree in August 2011 and is now with Amazon.com. Dr. Ling has been funded by an Alumni Fellowship at the University of Florida and has received his Ph.D. degree in August 2011 and is now with Mathworks. Dr. Roberts has been funded by a SMART fellowship and has received his Ph.D. degree in May 2010 and he is now working for the U.S. Army. Professor Stoica is funded by several funding agencies in Sweden and Europe. This team of researchers exchanges ideas and collaborates on joint journal and conference papers.

WORK COMPLETED

At the probing signal generation and transmission phase, we have focused on using cyclic algorithm-new (CAN) to synthesize probing sequences with good aperiodic autocorrelation and unimodular properties for the active sonar applications. CAN is based on the fast Fourier transform (FFT) and is applied for the minimization of the integrated sidelobe level (ISL) metric, which is of particular interest in active sonar systems. We compared the properties of the CAN sequences with those of two other popular sequences, namely the pseudo random noise (PRN) sequences and random phase (RP) sequences. Due to the optimization employed in the design of the CAN sequence, the sidelobes on the zero-Doppler line are significantly suppressed by the CAN sequence.

Moreover, we have extended CAN to efficiently generate unimodular sequence sets with good auto- and cross-correlations properties by exploiting FFTs. The extended algorithm can be used for the design of unimodular sequence sets with essentially zero auto-correlation sidelobes and zero cross-correlations in a specified time lag zone, as well as of sequence sets with good correlations over all time lags. These algorithms can start from random phase initializations and can generate many different sequence sets (including very long sequence sets) possessing similarly good correlation properties.

At the signal processing stage at the receiver, we have considered novel receiver design techniques to improve the overall performance of the active sonar system and to compensate for the deficiencies in waveform synthesis. We have developed two adaptive receiver designs, namely the iterative adaptive approach (IAA) and the sparse learning via iterative minimization (SLIM) method. Both approaches can work with even a signle snapshot and the array can be arbitrary. Both approaches outperform the classical data-independent matched filter methods significantly. Moreover, as a Bayesian signal recovery approach, the SLIM algorithm gives the *a posteriori* distribution of the target amplitudes. This information could be used for enhanced target detection and automatic target recognition.

We have also investigated the computational issues of SLIM and introduced a fast implementtion of the algorithm. In the active sonar problem, the steering matrix, which consists of the time-delayed and Doppler-scaled sequences, has a rich structure. We exploited the structure in the steering matrix, and make the matrix-vector multiplication computationally efficient by using the fast Fourier transform (FFT). Moreover, we apply the conjugate gradient (CG) method to transform the inversion of a matrix into a series of matrix-vector multiplications.

During the past year, we have focused on developing adaptive signal processing techniques in a multistatic active sonar system that employs multiple trnasmitters and multiple receivers. In the presence of severe interferences, as encountered in multistatic active sonar, the multiple simultaneously transmitted probing sequences act as interferences to one another, making the matched filter based receiver ineffective. In these cases where the problem is no longer noise limited, but rather interference limited, advanced adaptive receiver designs, such as IAA and SLIM, become necessary. In a multistatic setup, both IAA and SLIM significantly outperform the conventional matched filter for target range-Doppler imaging and interference suppression.

RESULTS

To demonstrate the effectiveness of using CAN for probing waveform design, the sequences generated by CAN were compared with PRN and RP sequences for active sonar applications. The RP sequences are unimodular with phased randomly distributed in $[0, 2\pi)$, while the PRN sequences are Gaussian random processes and are not restricted to be unimodular. The auto-correlation functions of a PRN sequence, an RP sequence and a CAN sequence (initialized by the PR sequence) are shown in Figures 1(a), 1(b), and 1(c), respectively. All the sequences are of length 400. The RP and CAN sequences are unimodular with amplitude 1. The PRN sequence is not unimodular and is normalized such that it has the same energy as the RP and CAN sequences. The ISL of the CAN sequence is 15.33 dB, while those of the PRN and RP sequences are 26.93 dB and 27.15 dB, respectively. In addition to the lower ISL, the peak sidelobe level (PSL) of the CAN sequence is -32.45 dB, while those of the PRN and RP sequences are -19.67 dB and -21.27 dB, respectively.

In Figures 2 (a)-(c), we show the ambiguity functions for the PRN, RP and CAN sequences, respectively. As can be seen from the images, the sidelobes of the PRN and RP sequences are of comparable level, which results in similar performance of the two sequences. For the CAN sequence, the sidelobes on the zero-Doppler line are significantly suppressed, due to the optimization employed in the design of the CAN sequence. However, the sidelobes of the CAN sequence in other parts of the ambiguity function are similar to those of the PRN and RP sequences. Therefore, sonar systems transmitting the CAN sequence and using the matched filter at the receiver will have a higher potential of detecting weak targets that might be missed by other systems transmitting PRN or RP sequences only when the targets occupy the same Doppler bin. Consider the example shown in Figure 3, where two targets separated in range by 95 m are to be detected by sonar systems transmitting PRN, RP and CAN sequences. The amplitude of the strong target is 1, while that of the weak one is 0.1. As can be seen from the figure, for both PRN and RP sequences, the weak target is missed due to the interferences from the strong target. However, the system transmitting a CAN sequence clearly indicates the presence of both targets and gives accurate estimates of the target echo levels. Figure 4 shows the 1-D cut of Figure 3 corresponding to the zero-Doppler line. As is clearly shown in the figure, the sidelobes of PRN and RP are so high that the weak target is buried by the leakage from the strong one. For the CAN sequence, the sidelobes are low enough for the weak target (which shares the same Doppler as the strong target) to be detected.

We have tested the effectiveness of using CAN waveform as probing pulses in active sonar applications. We use the sonar simulation toolset (SST) to simulate the active sonar system and the practical oceanic environment in which the system works (by collaborating with Dr. Michael S. Datum of the Applied Physical Sciences Corp.).

First, we consider a bistatic active sonar system. The simulation geometry is shown in Figure 5, where the receiver is 2 km away from the transmitter, which sends out a CAN sequence into the region of interest. A target, located on the perpendicular bisector of the segment connecting the transmitter and the receiver, is 6 km away from the receiver and moves at a radial velocity of 2 knots. In the simulation, the length of the CAN sequence is 400. The bandwidth of the transmitted sequence is 200 Hz, and the carrier frequency is 900 Hz. The sampling rate at the transmitter is 8000 Hz and the transmitted sequences are of duration 2 seconds. At the receiver end, independent ambient noise and a Gaussian reverberation, here dominated by bottom scatterers, are considered. The sea bottom depth is 200 m and the level of the reverberation drops off with the distance from the transmitter and receiver. The received sequences were of duration 12 seconds and sampled at the same sampling rate of 8000 Hz. The length of the received sequence is M = 2400. The beamformed output was processed using MF, IAA and the fast implementation of SLIM (fast-SLIM). The considered Doppler range covered a radial velocity from -4 knots to 4 knots, with positive values denoting an approaching target. The Doppler step is 0.2 knots, and the number of Doppler bins is 41.

Figures 6(a), 6(b), and 6(c) show the range-Doppler images of the simulated SST data formed with MF, IAA, and fast-SLIM. The images produced by the matched filter show the presence of a large number of high sidelobes, in both dimensions of range and Doppler. This is because the matched filter response to a transmitted sequence is characterized by the ambiguity function, the volume underneath the square of which is a constant for different sequences with the same energy. However, despite the high sidelobes of the matched filter images and hence despite a potentially high false alarm, the presence of the target is clearly indicated, with correct location and velocity estimates. Comparing the images generated using the adaptive receiver designs with that of the matched filter, it is clear that both IAA and SLIM have superior performance over the matched filter. It is evidenced by Figure 6(b) that the sidelobes are significantly suppressed in the IAA image, giving much cleaner image than the matched filter. In the image given by fast-SLIM, all pixels are estimated as zeros except the target, thus the results are sparse representations of the region of interest. With the fast implementations, the computing time for fast-SLIM reduces to about 75 seconds while that for the origianal SLIM is about two hours. Another benefit of SLIM is that it provides us with the *a posteriori* PDF of the estimates, which can be utilized for the investigation of the statistical properties of the estimates, as well as for the automatic target recognition.

We have also considerd a more challanging three-target example. The three targets are closely spaced with each other. One target is 6 km away from the receiver and moves at a radial velocity of 0.38 knots. The other two targets are 5.9 km away form the receiver and move at a radial velocity of 0 knots and 0.38 knots, respectively. The range-Doppler images formed using MF, IAA, and fast-SLIM are shown in Figures 7(a), 7(b), and 7(c), respectively. Both IAA and fast-SLIM significantly outperforms the matched filter. The sidelobes are significantly suppressed in the IAA and fast-SLIM images. In the image given by fast-SLIM, all three targets are represented sparsely. Moreover, fast-SLIM has a higher resolution than IAA.

Then we consider a multistatic active sonar system equipped with two stationary transmitters and two stationary receivers (by stationary, we mean that their positions are fixed during the sensing operation). The system geometry is illustrated in Figure 8. The coordinate vectors of the two receivers Rx1 and Rx2 are (2000, 0) and (0, 2000), respectively (the unit of distance is meter). Two transmitters, Tx1 and Tx2, are located at (0, 0) and (2000, 2000), respectively, and transmit two random phase (RP) sequences simultaneously. The RP sequences are unimodular with phases independently and uniformly distributed over $[0, 2\pi)$. There are two targets moving in the filed of view. The first target, located at

(1000, 995), is moving at -135° (with respect to east) at a radial velocity of 1.8 knots. The second target is located at (1050, 965) and is moving at -90° at 2 knots knots. The Doppler bins correspond to Doppler scaling factors ranging from 0.9976 to 1.0024 with a step size of 0.0003. The zero-mean white Gaussian noise with a power of −10 dB is added to the received measurements. The system parameters are given in Table I.

The receiver outputs are processed using the conventional matched filter (MF), IAA, and SLIM. The intensity of the range-Doppler images is normalized so that the peak is at 0 dB and is clipped at −40 dB. Figure 9 shows the IAA image with respect to Tx1 formed by Rx1. In Figure 9, the 0 dB peak corresponds to the direct blast, the signals propagating directly from the transmitters to the receivers (intensity-wise, the direct blasts tend to be much stronger than the target reflections). This peak corresponds to a range estimate of approximately 2 km and a Doppler scaling factor estimate of 1. These estimates are in line with the facts that the distance between Tx1 and Rx1 is 2 km and the direct blast is not subject to Doppler scaling in the case of stationary transmitter and receiver platforms. For the sake of clarity and also due to the fact that the location of the direct blast in the range-Doppler images is predictable given the positions of the transmitters and receivers, the range-Doppler images presented henceforth focus on the target locations only. Figure 10 shows the range-Doppler images produced by the three receiver filter designs. The MF images with respect to the two transmitters formed by Rx1 (Rx2) are shown in Figures 10(a) and 10(b) (Figures 10(c) and 10(d)), respectively. One observes that due to the mutual interferences of the target reflections and strong direct blasts, the MF images are mired with background noise, making it difficult to detect the two targets.

The range-Doppler images produced by IAA and SLIM are shown in Figures 10(e)–10(h) and Figures 10(i)–10(l), respectively. We can see that both IAA and SLIM possess excellent interference suppression capabilities and produce much sharper images than MF. In particular, IAA does not enforce sparsity and the sidelobe levels of the IAA image are mostly below −25 dB. In contrast, SLIM, for being a sparse signal recovery algorithm, gives very clean target range-Doppler images. Moreover, for both adaptive receiver designs, the range and Doppler estimates of both targets are quite accurate.

Next, for comparison purposes, we assess the performance of a conventional active sonar imaging approach, where both receivers have the perfect knowledge of one of the pings, but not both. Specifically, if both receivers know the ping transmitted by Tx1 only, then the target echoes in response to the ping transmitted by Tx2 can be treated as unknown interferences. The resulting range-Doppler images produced by IAA and SLIM are shown in Figures 11(a), 11(c) and Figures 11(e), 11(g), respectively. If both receivers know the ping transmitted by Tx2 only, then the corresponding images are shown in Figures 11(b), 11(d) and Figures 11(f), 11(h), respectively. Note that the MF images are not shown here because they are identical to Figures 10(a)–10(d). The two different imaging schemes produce the same MF images since MF is a data-independent approach. The interference suppression advantage of multistatic adaptive active sonar imaging over its conventional counterpart is clearly demonstrated by comparing Figures 11(a)–11(d) with Figures 10(e)–10(h) and Figures 11(e)–11(h) with Figures 10(i)–10(l). Indeed, the incorporation of the knowledge of both pings for range-Doppler imaging makes it possible for IAA and SLIM to significantly improve the accuracy of the range-Doppler images for both receivers.

To summarize the analysis made previously, MF is the simplest design with the highest computational efficiency. MF, however, provides poor resolution and suffers from high sidelobe level problems. Moreover, MF becomes useless in the presence of strong mutual interferences and direct blasts. Both IAA and SLIM possess excellent capabilities for interference suppression with much improved

resolution as compared to MF. IAA does not enforce sparsity, whereas SLIM is a sparse signal recovery algorithm. Complexity-wise, similarly to the single transmitter single receiver case, the fast implementation of SLIM is significantly faster than IAA in a multistatic setup.

IMPACT/APPLICATIONS

The littoral submarines are small, quiet, and non-nuclear, making active sonar an essential technology needed for their detection. Enhancing the multistatic active sonar network's capability through innovative waveform synthesis and receive filter design is critical to improving the Navy's ability to conduct anti-submarine warfare.

The novel unimodular probing waveform we synthesize is hard to guess by the foe since the phase of each sample of the probing sequence is anywhere between 0 and 2π. This facilitates covert sensing. Moreover, the Doppler sensitive nature of the probing waveform we synthesize obviates the need to transmit two separate sequences, with one to achieve good range resolution and another to yield good Doppler resolution. Using our Doppler sensitive probing waveforms, we can achieve both good range resolution and good Doppler resoltuion simutaneously.

By using data-adaptive receive filters to process the received signals, the sidelobe problems of Doppler sensitive probing waveforms can be mitigated. Indeed, the range-Doppler images formed by using the adaptive receivers we devise possess low sidelobe level and high resolution properties.

By using the SST data sets to demonstrate the effectiveness of our probing waveform synthesis and receive filter design techniques, we have convincingly demonstrated their potentials for anti-submarine warfare applications. In-water experimentations are needed to further demonstrate the utility of the techniques.

In a multistatic active sonar system that employs multiple transmitters and multiple receivers, we have shown that reliable adaptive receiver filters, via enhancing resolution and reducing sidelobe levels of the so-obtained range-Doppler images, significantly enhance the target detection ability.

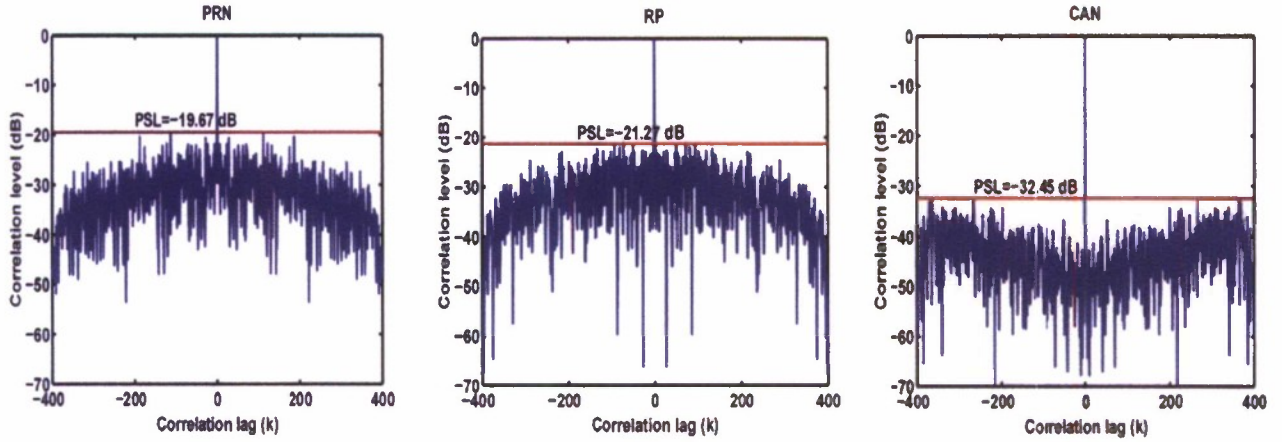

Figure 1. Auto-correlation functions of (a) a PRN sequence, (b) an RP sequence, and (c) a CAN sequence. All sequences are of length 400 and have equal energy.

[graph: The integrated sidelobe level (ISL) and the peak sidelobe level (PSL) of the CAN sequence are over 10 dB less than those of PRN and RP sequences.]

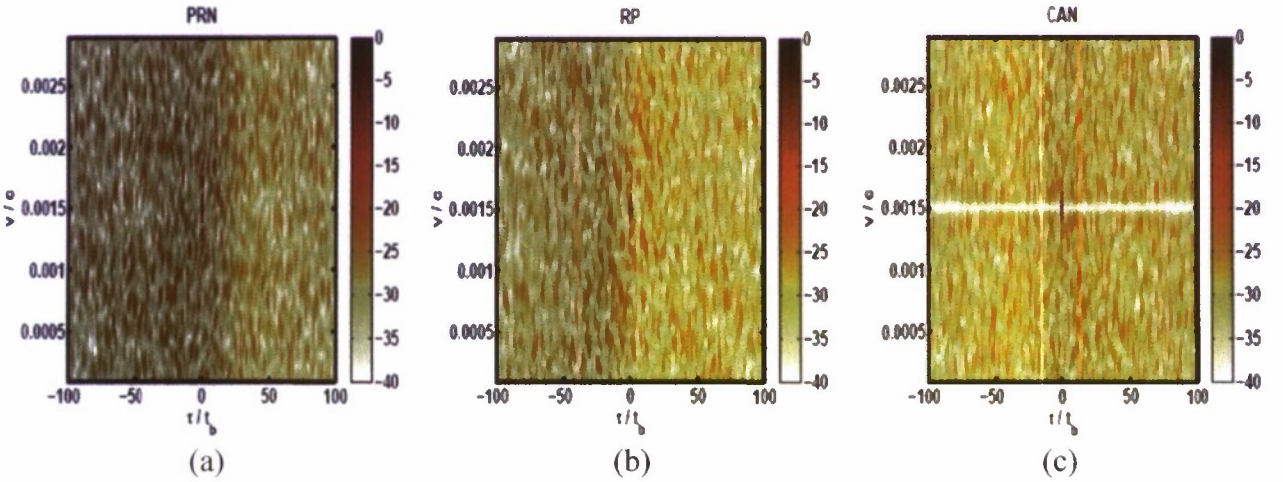

Figure 2. Ambiguity functions of (a) a PRN sequence, (b) an RP sequence, and (c) a CAN sequence.

[graph: For the CAN sequence, the sidelobes on the zero-Doppler line are significantly suppressed, due to the optimization employed in the design of the CAN sequence.]

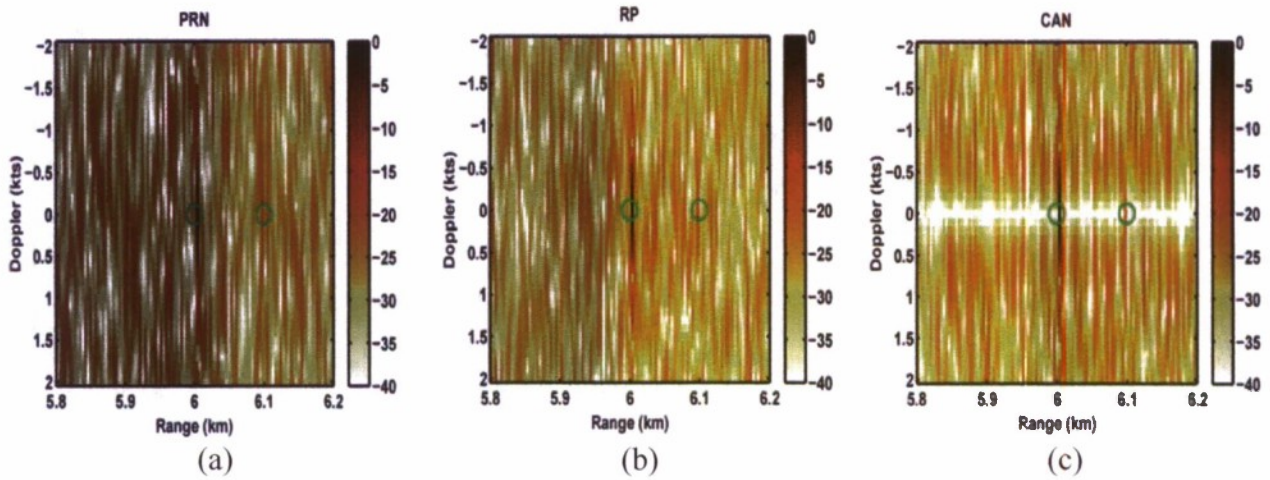

Figure 3. Target detection and range-Doppler imaging via matched filtering at the receiver while transmitting (a) a PRN sequence, (b) an RP sequence, and (c) a CAN sequence. Circles indicate the true target range and Doppler location.

[graph: The system transmitting a CAN sequence clearly indicates the presence of both targets and gives accurate estimates of the target echo levels.]

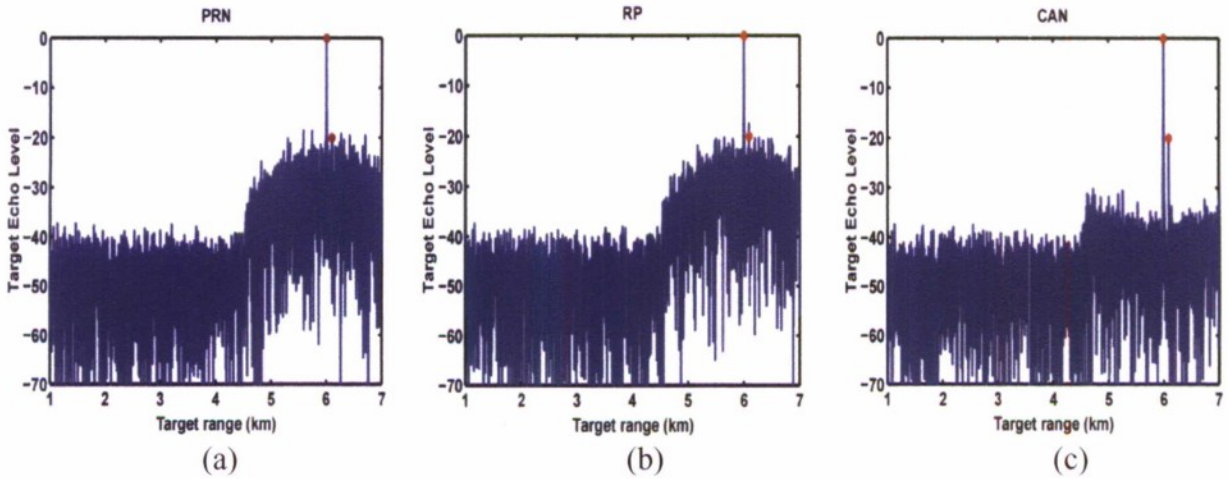

Figure 4. Target echo level versus range obtained using (a) a PRN sequence, (b) an RP sequence, and (c) a CAN sequence. Bullets indicate the true target echo level and location.

[graph: The sidelobes of PRN and RP are so high that the weak target is buried by the leakage from the strong one. However, the sidelobes for the CAN sequence are low enough for the weak target to be detected.]

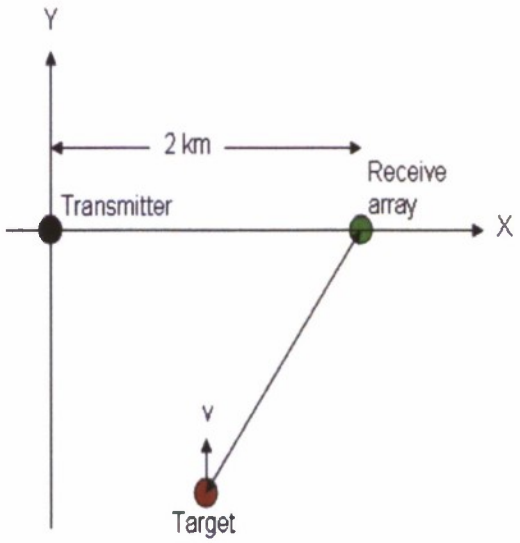

Figure 5. The simulation geometry.

[graph: The receiver is 2 km away from the transmitter, which sends out a CAN sequence into the region of interest. A target, located on the perpendicular bisector of the segment connecting the transmitter and the receiver, is 6 km away from the receiver and moves at a radial velocity of 2 knots.]

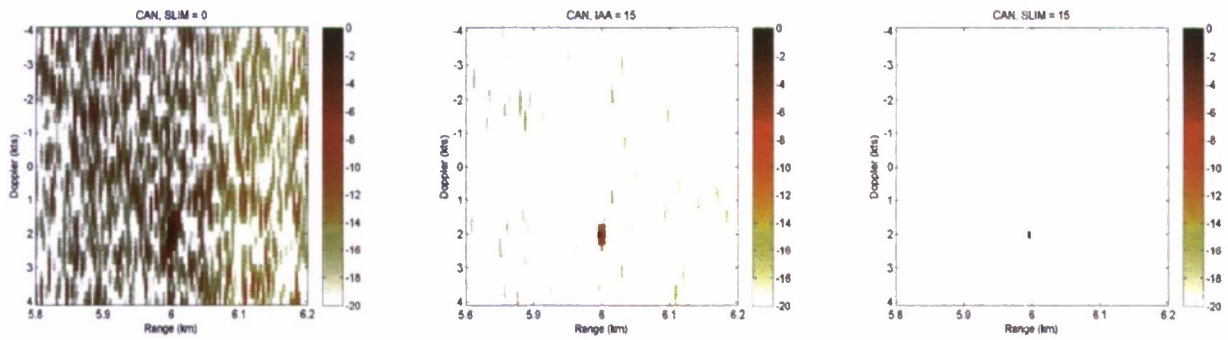

Figure 6. Range-Doppler images of SST data formed with (a) MF, (b) IAA, and (c) fast-SLIM. A target is 6 km away from the receiver and moves at a radial velocity of 2 knots.

[graph: Both IAA and fast-SLIM have superior performance over the matched filter. The sidelobes are significantly suppressed in the IAA image, giving much cleaner image than the matched filter. In the image given by fast-SLIM, all pixels are estimated as zeros except for the target, thus the results are sparse representations of the region of interest.]

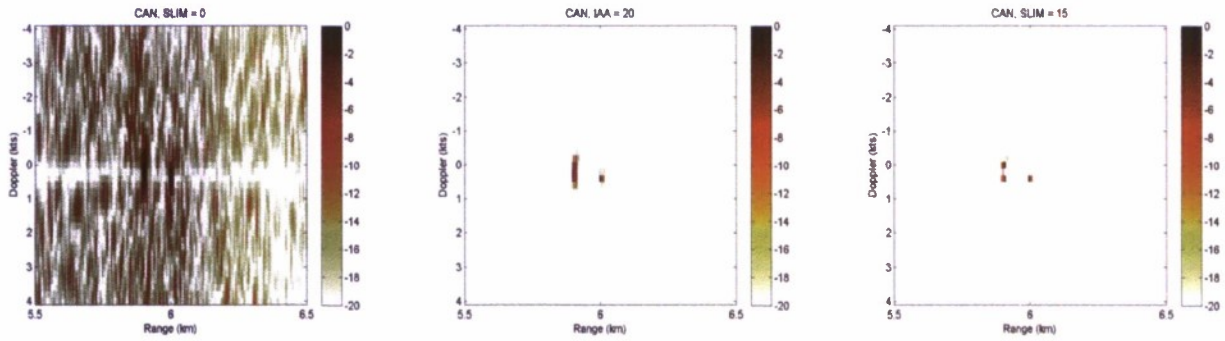

Figure 7. Range-Doppler images of SST data formed with (a) MF, (b) IAA, and (c) fast-SLIM. There are three targets. One target is 6 km away from the receiver and moves at a radial velocity of 0.38 knots. The other two targets are 5.9 km away form the receiver and move at a radial velocity of 0 knots and 0.38 knots, respectively.

[graph: Both IAA and fast-SLIM significantly outperform the matched filter. The sidelobes are significantly suppressed in the IAA and fast-SLIM images. In the image given by fast-SLIM, all three targets are represented sparsely. Fast-SLIM provides higher resolution than IAA.]

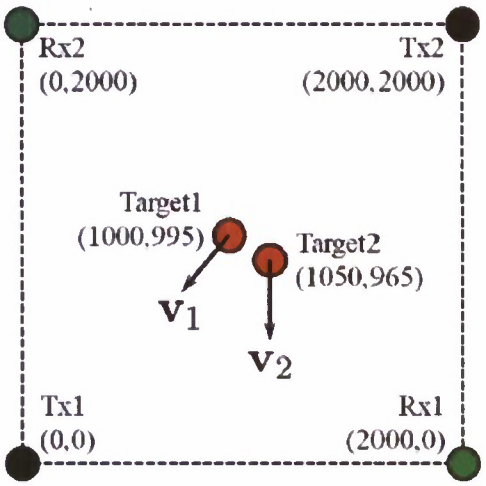

Figure 8. The simulation geometry.

[graph: The coordinate vectors of the two receivers Rx1 and Rx2 are (2000, 0) and (0, 2000), respectively (the unit of distance is meter). Two transmitters, Tx1 and Tx2, are located at (0, 0) and (2000, 2000), respectively. There are two targets moving in the filed of view. The first target, located at (1000, 995), is moving at -135° (with respect to east) at a radial velocity of 1.8 knots. The second target is located at (1050, 965) and is moving at -90° at 2 knots.]

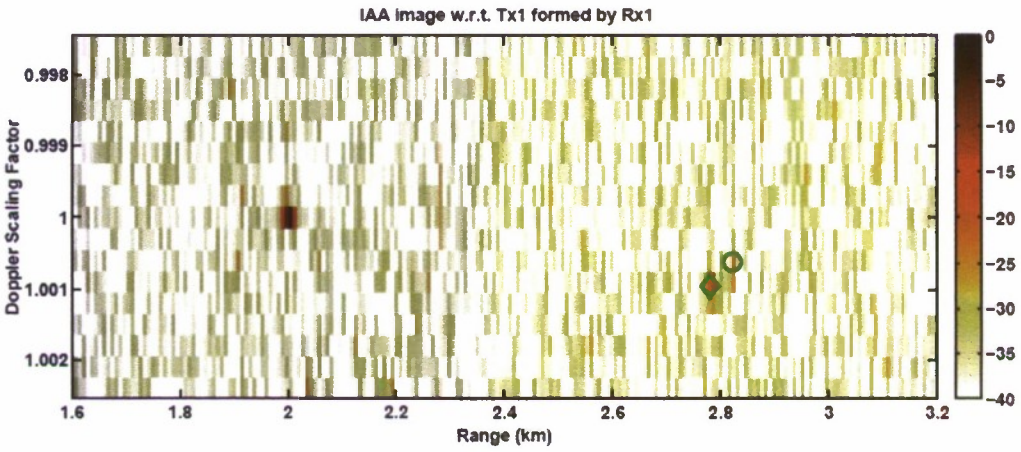

Figure 9. Range-Doppler images produced by a multistatic active sonar system using IAA. Circle and diamond indicate the true locations of the first and second targets, respectively. The 0 dB peak at 2 km range corresponds to the direct blast from Tx1.

[graph: The three peaks in the IAA image with respect to Tx1 formed by Rx1, correspond to the direct blast and the two targets in the field of view.]

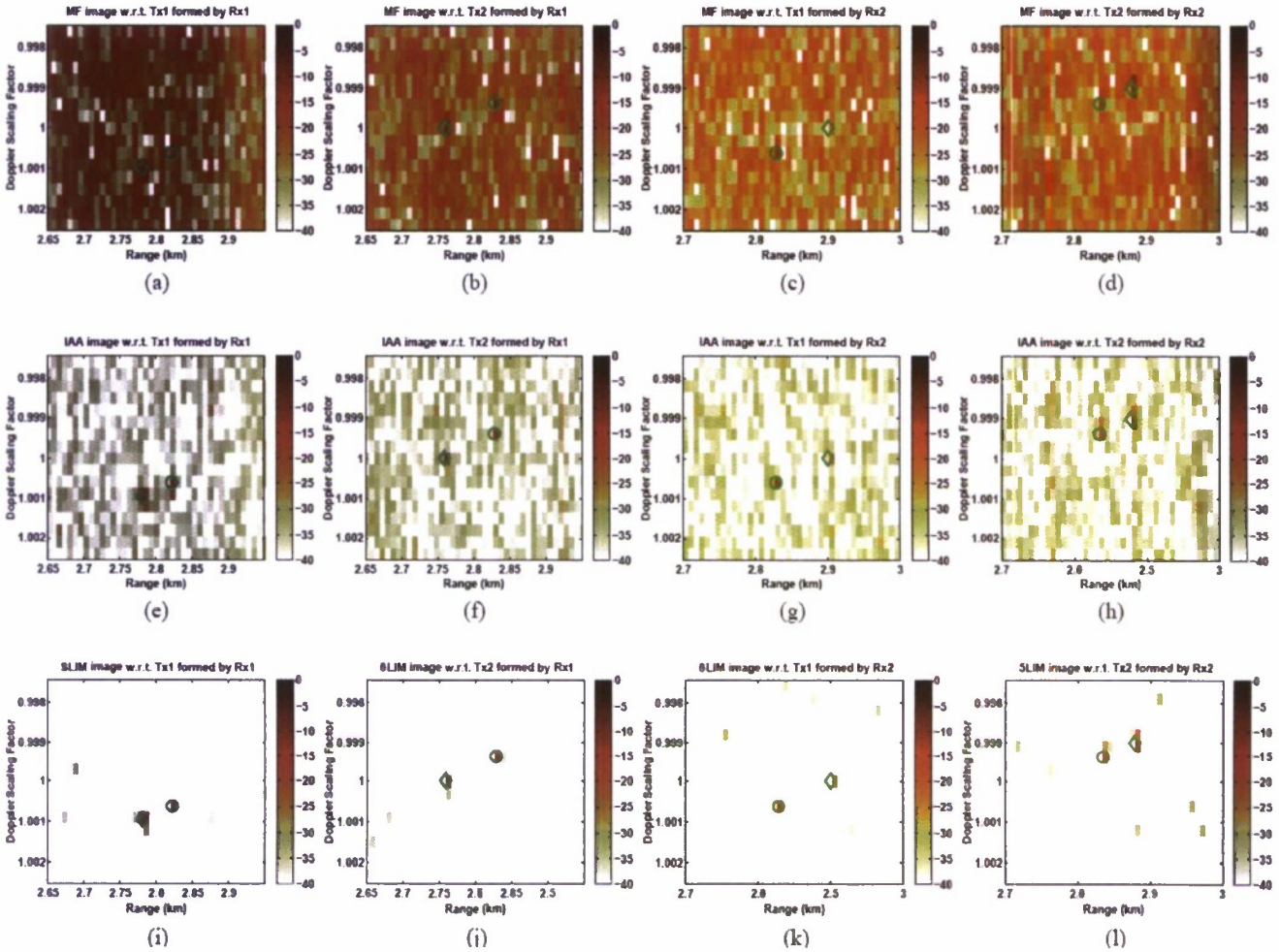

Figure 10. Range-Doppler images produced by a multistatic active sonar system using various receiver filters. Circles and diamonds indicatethe true locations of the first and second targets, respectively.

[graph: IAA and SLIM prossess excellent interference suppression capabilities and produce much sharper images than MF. For both adaptive receiver designs, the range and Doppler estimates of both targets are quite accurate.]

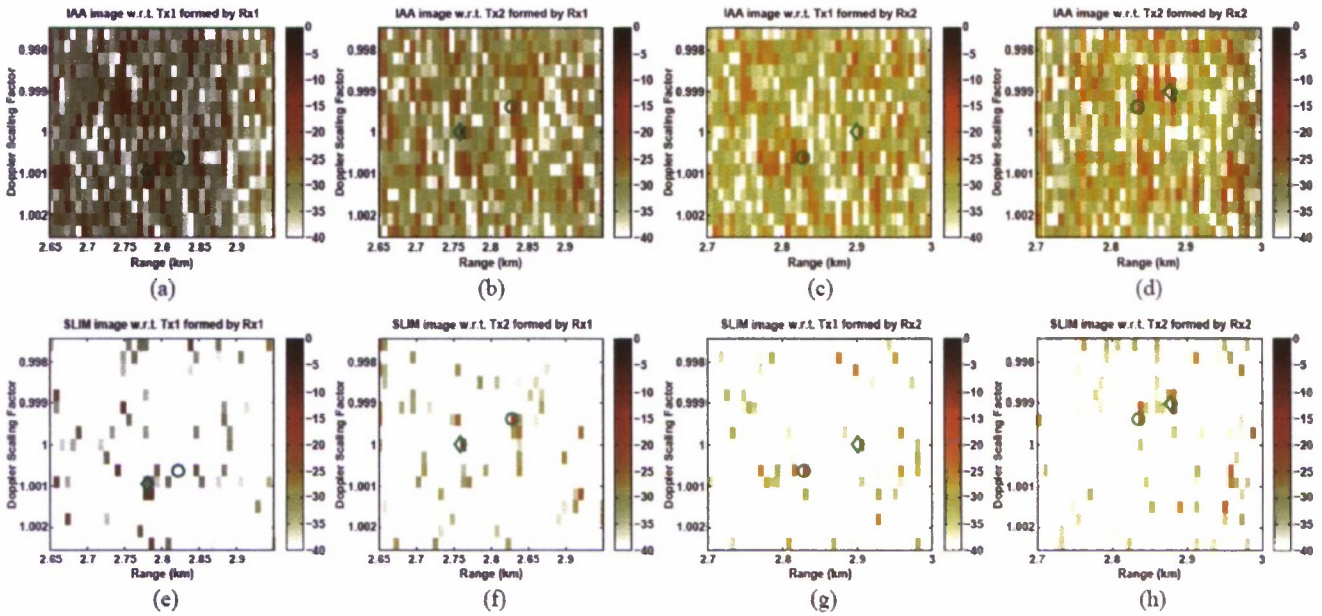

Figure 11. Range-Doppler images produced by a conventional active sonar imaging approach. Circles and diamonds indicate the true locations of the first and second targets, respectively.

[graph: The incorporation of the knowledge of both pings form range-Doppler imaging makes it possible for IAA and SLIM to significantly improve the accuracy of the range-Doppler images for both receivers, see Figure 3.]

Table I. The system parameters.

underwater sound speed	1500 m/s or 2915.77 knots
length of the transmitted pings	400
bandwidth of the transmitted pings	200 Hz
number of Doppler bins	17
carrier frequency	900 Hz
sampling frequency at transmitter and receiver	8000 Hz
duration of the transmitted pings	2 s

TRANSITIONS

We have provided several CAN sequences to Dr. Michael S. Datum of the Applied Physical Sciences Corporation. He has used some of the sequences as active sonar probing sequences and generated simulated datasets for ASW scenarios using the sonar simulation toolset (SST). The simulated datasets

will be shared with us for further analysis. We plan to use the SST simulated datasets to evaluate the performance of our receive filter designs. We plan to publish joint papers based on our discoveries. This has been a fruitful collaboration.

We have also recently sent our probing waveform synthesis papers to Dr. James Alsup (alsup@cox.net) and our IAA papers to Dr. Roy Streit (streit@metsci.com).

RELATED PROJECTS

NONE.

PUBLICATIONS

Journal Publications

J. Ling, and J. Li, "Adaptive range-Doppler imaging and target parameter estimation in multistatic active sonar systems," *IEEE Journal of Oceanic Engineering.* [submitted]

M. Xue, L. Xu, and J. Li, "IAA Spectral Estimation: Fast Implementation Using the Gohberg-Semencul Factorization," *IEEE Transactions on Signal Processing*, Vol. 59, No. 7, pp. 3251 – 3261, July 2011. [published, refereed].

J. Ling, J. Li, P. Stoica, and M. Datum, "Probing waveforms and adaptive receivers for active sonar," *Journal of the Acoustical Society of America*, vol. 129, no. 6, pp. 3640-3651, June 2011. [published, refereed].

X. Tan, W. Roberts, J. Li, and P. Stoica, "Sparse Learning via Iterative Minimization with Application to MIMO Radar Imaging," *IEEE Transactions on Signal Processing*, Vol. 59, No. 3, pp. 1088-1101, March 2011. [published, refereed].

W. Roberts, L. Xu, J. Li, and P. Stoica, "Sparse antenna array design for MIMO active sensing applications," *IEEE Transactions on Antennas and Propagation*, Vol. 59, No. 3, pp. 846-858, March 2011. [published, refereed].

H. He, P. Stoica and J. Li, "Wideband MIMO Systems: Signal Design for Transmit Beampattern Synthesis", *IEEE Transactions on Signal Processing*, Vol. 59, No. 2, pp. 618 – 628, February 2011. [published, refereed].

P. Stoica, P. Babu, and J. Li, "New Method of Sparse Parameter Estimation in Separable Models and Its Use for Spectral Analysis of Irregularly Sampled Data," *IEEE Transactions on Signal Processing*, Vol. 59, No. 1, pp. 35 – 47, January 2011. [published, refereed].

X. Tan and J. Li, "Cooperative Positioning in Underwater Sensor Networks," *IEEE Transactions on Signal Processing*, vol. 58, no. 11, pp. 5860-5871, November 2010. [published, refereed].

J. Ling, H. He, J. Li, W. Roberts, and P. Stoica, "Covert Underwater Acoustic Communications," *Journal of the Acoustical Society of America*, vol. 128, no. 5, pp. 2898-2909, November, 2010. [published, refereed].

W. Roberts, H. He, J. Li and P. Stoica, "Probing Waveform Synthesis and Receiver Filter Design," *IEEE Signal Processing Magazine*, vol. 27, no. 4, pp. 99-112, July 2010. [published, refereed].

X. Tan and J. Li, "Range-Doppler Imaging via Forward-Backward Sparse Bayesian Learning," *IEEE Transactions on Signal Processing*, Vol. 58, No. 4, pp. 2021-2025, April 2010. [published, refereed].

X. Tan and J. Li, "Computationally Efficient Sparse Bayesian Learning via Belief Propagation," *IEEE Transactions on Signal Processing*, vol. 58, no. 4, pp. 2010-2021, April, 2010. [published, refereed].

H. He, P. Stoica and J. Li, "On aperiodic-correlation bounds," *IEEE Signal Processing Letters*, vol. 17, no. 3, pp. 253-256, March 2010. [published, refereed].

P. Stoica, H. He, and J. Li, "Sequence sets with optimal integrated periodic correlation level," *IEEE Signal Processing Letters*, vol. 17, no. 1, pp. 63-66, January 2010. [published, refereed].

H. He, P. Stoica, and J. Li, "Designing unimodular sequence sets with good correlations -- Including an application to MIMO radar," *IEEE Transactions on Signal Processing*, vol. 57, no. 11, pp. 4391-4405, November 2009. [published, refereed].

P. Stoica, H. He, and J. Li, "On designing sequences with impulse-like periodic correlation," *IEEE Signal Processing Letters*, vol. 16, no. 8, pp. 703-706, August 2009. [published, refereed].

P. Stoica, H. He, and J. Li, "New algorithms for designing unimodular sequences with good correlation properties," *IEEE Transactions on Signal Processing*, vol. 57, no. 4, pp. 1415-1425, April 2009. [published, refereed].

Conference Publications

J. Ling and J. Li, "Multistatic adaptive active sonar imaging and target tracking," *Proceedings of IEEE Oceans Conference*, Santander, Spain, June 2011. [published, refereed].

M. Xue, L. Xu, J. Li, and P. Stoica, "IAA Spectral Estimation: Fast Implementation Using the Gohberg-Semencul Factorization," *IEEE International Conference on Acoustics, Speech and Signal Processing*, Prague, Czech Republic, May 22-27, 2011. [published, refereed].

H. He, P. Stoica, and J. Li, "On Synthesizing Cross Ambiguity Functions," *IEEE International Conference on Acoustics, Speech and Signal Processing*, Prague, Czech Republic, May 22-27, 2011. [published, refereed].

X. Tan and J. Li, "Cooperative positioning in underwater sensor networks," *Proceedings of the MTS/IEEE Oceans Conference*, Seattle, WA, September 2010. [published, refereed].

Z. Chen, J. Li, X. Tan, H. He, B. Guo, P. Stoica, and M. Datum, "On probing waveforms and adaptive receivers for active sonar," *Proceedings of the MTS/IEEE Oceans Conference*, Seattle, WA, September 2010. [published, refereed].

H. He, P. Stoica, and J. Li, "Wideband MIMO Waveform Design for Transmit Beampattern Synthesis," *IEEE 5th International Waveform Diversity & Design Conference*, Niagara Falls, Canada, August 8-13, 2010. [published, refereed].

H. He, P. Stoica, and J. Li, "Waveform design with stopband and correlation constraints for cognitive radar," *The 2nd International Workshop on Cognitive Information Processing* (invited), Elba Island, Italy, June 2010. [published].

H. He, D. Vu, P. Stoica, and J. Li, "Construction of unimodular sequence sets for periodic correlations," *The 2009 Asilomar Conference on Signals, Systems and Computers* (invited), Pacific Grove, CA, USA, November 1-4, 2009. [published].

X. Tan and J. Li, "Computationally Efficient Sparse Bayesian Learning via Belief Propagation," *The 2009 Asilomar Conference on Signals, Systems and Computers*, Pacific Grove, CA, USA, November 1-4, 2009. [published, refereed].

W. Roberts, H. He, X. Tan, M. Xue, D. Vu, J. Li, and P. Stoica, "Probing Waveform Synthesis and Receive Filter Design for Active Sensing Systems," *2009 SPIE Defense, Security, and Sensing Conference* (invited), Orlando, Florida, April 13-17, 2009. [published].

HONORS/AWARDS/PRIZES

The following paper received the **Top 10 Best Student Paper Award:**

H. He, P. Stoica, and J. Li, "Waveform design with stopband and correlation constraints for cognitive radar," The 2nd International Workshop on Cognitive Information Processing, Elba Island, Italy, June 2010.

The following paper received the **Lockheed-Martin Best Student Paper Award**:

W. Roberts, H. He, X. Tan, M. Xue, D. Vu, J. Li, and P. Stoica, "Probing Waveform Synthesis and Receive Filter Design for Active Sensing Systems," *2009 SPIE Defense, Security, and Sensing Conference* (invited), Orlando, Florida, April 13-17, 2009.